Development and testing of the gravitational wave antenna MiniGRAIL in its full-featured configuration

Usenko, O.

Chapter 1

Principles of operation of a spherical gravitational wave antenna MiniGRAIL

Introduction

The concept of a spherical gravitational wave detector was already suggested in the early seventies by [14]. Spherical detectors have a number of advantages:

- Omni-directionality. Due to its symmetric nature, a spherical detector is the only detector of gravitational waves with isotropic sky coverage and the capability of finding the location of the source. Both laser interferometers and bar detectors are unable to do this with just one detector.

- Ability to determine direction and polarization $h+$, $h\times$ of an incoming gravitational wave (in a multiple transducers configuration). A single sphere is capable of determining the source direction and polarization, because it has five degenerate modes of oscillation that interact with gravitational waves. An observatory consisting of two spherical detectors could give the exact location of the source, which makes it possible to determine the velocity of the gravitational waves and also decreases the false alarm rate.

- Large cross section compared to a bar detector. A sphere has a larger mass than a bar resonating at the same frequency and because it is equally sensitive for all directions and polarizations it has an energy cross section about 50 times larger than a bar of the same material.

- Since a spherical detector is quite compact, compared to other types of detectors, it is possible to fit it in a conventional type of cryostat. As a consequence such

a detector is relatively cheap and can be installed and operated in a typical research laboratory by a small scientific group.

- Toroidal modes of the sphere could possibly be used as vetoes for non-GW signals. Since the gravitational waves only excite the quadrupolar modes of the sphere, it is possible to use the signal from the other modes as a veto [15].

However, there are some practical problems in operating a spherical detectors. As we will describe below, the sphere has five vibrational modes that couple to gravitational waves. Hence a set of at least five(or even six, like in MiniGRAIL) mechanical resonators(transducers) followed by six low noise amplifiers is required. Six transducers, coupled to the sphere modes will result in at least 11 resonant modes which make the analysis complicated. Moreover, the advantages if the spherical detector come at a price of its reliability. A failure rate of 10% for a single read-out channel would result in only $\approx 50\%$ success rate if all six channels have to be operational. Fortunately, as we would see further in this thesis, it is possible to operate the detector with less than 6 working read-out channels without catastrophic degradation of its performance.

In this chapter we give a brief introduction into the theory, needed to understand the gravitational wave detection. A detailed description of classical theory of gravitational waves is out of scope of this thesis, but can be found for instance in [16] [17] or [18] A more specific and shorter explanation from the point of view of spherical gravitational wave detector can be found in [19, 20, 21, 22, 23].
In the second part of this chapter we will also give a description of an actual MiniGRAIL setup, detection method and expected sensitivity.

1.1 Interaction of gravitational waves with a physical body

In general relativity gravitational waves are ripples in the curvature of space-time that propagate with the speed of light. For any practical source of gravitational waves they can be described as small perturbation $h_{\mu\nu}$ of a flat space-time with a metric $\eta_{\mu\nu} = diag(-1, 1, 1, 1)$("linearized gravitational waves approximation")[17][24]:

$$g_{\mu\nu} = \eta_{\mu\nu} + h_{\mu\nu}, \text{ where } |h_{\mu\nu}| \ll 1, \tag{1.1}$$

Away from the source we can choose a gauge where gravitational wave metric perturbation $h_{\mu\nu}$ can be reduced to h_{ij}^{TT}, containing only spatial components. The superscript TT denotes a *transverse-traceless* gauge (TT gauge)[18]. A physical meaning of a TT gauge is that the gravitational wave is described as a plain wave perpendicular to propagation direction and the particle that was at rest before the wave came would remain at rest after the wave has passed.

We can further simplify the h_{ij} tensor by choosing a reference frame with the origin of coordinate system in the center of mass of the detector, and the z-axis oriented along the direction of incoming gravitational wave - a *wave-frame*. In a wave-frame, a time dependent $h_{ij}(t)$ tensor can be written as

$$h_{i'j'}(t) = \begin{bmatrix} h'_+(t) & h'_\times(t) & 0 \\ h'_\times(t) & -h'_+(t) & 0 \\ 0 & 0 & 0 \end{bmatrix} \tag{1.2}$$

where $h'_+ \equiv h_{x'x'} = -h_{y'y'}$ and $h'_\times \equiv h_{x'y'} = h_{y'x'}$ are the amplitudes of two gravitational wave polarizations, called the plus and cross polarizations. Primed indexes denote the wave-frame.

The force lines of two polarizations are shown on figure 1.1. A plus polarization would deform a ring of test masses into an ellipse with axes along with x and y directions. A cross polarization deforms a ring at $\frac{\pi}{4}$ angle to x and y directions.

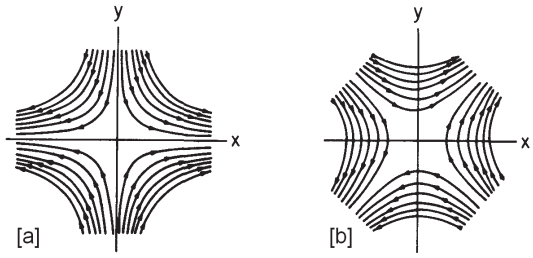

Figure 1.1**:** Force lines of *plus*[a] and *cross*[b] polarized gravitational wave propagating in *z-axis* direction[18]

The detector is better described in the reference frame, with the center being also located in the center of mass of the detector and the *z-axis* aligned with the local vertical, a *lab-frame* or *detector-frame*

In the lab-frame frame the physical effect of a passing gravitational wave is to produce a Newtonian force on a test particle. For a material with a density ρ at coordinate location x_i a time dependent force density $f^{GW}(x,t)$ is related to the metric perturbation by

$$f_i^{GW}(\mathbf{x},t) = \frac{1}{2}\rho \sum_j \frac{\partial^2 h_{ij}(t)}{\partial t^2} x_j \tag{1.3}$$

This is a remarkable result, as from this point on the study of the interaction between the gravitational wave and the detector will not require involving general relativity.

1.1.1 Coupling of gravitational waves to the sphere

The equation (1.3) can be rewritten in spherical coordinates. For a spherical detector it is convenient to describe the angular part with five second order spherical harmonics $Y_{2m}(\theta,\phi)$ $(m = 1 \ldots 5)$ [20]

$$\mathbf{Y}_{2m} = \sqrt{\frac{15}{16\pi}} \begin{pmatrix} \cos 2\varphi \sin^2\theta \\ \sin 2\varphi \sin^2\theta \\ \sin\varphi \sin 2\theta \\ \cos\varphi \sin 2\theta \\ \frac{1}{\sqrt{3}}(3\cos^2\theta - 1) \end{pmatrix} \tag{1.4}$$

The resulting time dependent expansion coefficients, $h_m(t)$, are called spherical amplitudes [20]. They are a complete and orthogonal representation of the Cartesian metric tensor $h_{ij}(t)$. They only depend on the two wave-frame amplitudes and the direction of propagation.

The conversion from a *wave-frame* to a *lab-frame* can be done by applying the rotation matrix. After the rotation, the spherical amplitudes in the lab-frame can be expressed in terms of the polarization amplitudes and the source direction:

$$\begin{aligned} \mathbf{h}_m &= \mathbf{T_V} \begin{pmatrix} h_+ \\ h_\times \end{pmatrix}, \\ \mathbf{T_V} &= \begin{pmatrix} \frac{1}{2}\left(1+\cos^2\beta\right)\cos 2\gamma & \cos\beta \sin 2\gamma \\ \frac{1}{2}\left(1+\cos^2\beta\right)\sin 2\gamma & \cos\beta\cos 2\gamma \\ \frac{1}{2}\sin 2\beta \sin\gamma & \sin\beta\cos\gamma \\ \frac{1}{2}\sin 2\beta\cos\gamma & \sin\beta\sin\gamma \\ \frac{1}{2}\sqrt{3}\sin^2\beta & 0 \end{pmatrix} \begin{pmatrix} \cos 2\alpha & \sin 2\alpha \\ -\sin 2\alpha & \cos 2\alpha \end{pmatrix}, \end{aligned} \tag{1.5}$$

where rotation angles β, γ and α follow standard Euler angles convention(see figure 1.2) - β is the angle between z' and z axis and γ is the angle between the line of nodes N and x axis [22]. Angle α shows the rotation around the wave-frame axis z' and gives the information about the gravitational wave polarization.

1.1.2 Modes of the Uncoupled Sphere

In this section we describe the interaction of the gravitational wave with a spherical antenna. The mechanics of a spherical antenna is described by ordinary elastic theory. Force, acting on elastic body will cause a deformation of $x = x_0 + u(x,t)$, where x_0 is the equilibrium position of a volume element. The equation of motion of an elastic body is

$$\rho\frac{\partial^2\mathbf{u}}{\partial t^2} = (\lambda+\mu)\nabla(\nabla\cdot\mathbf{u}) + \mu\nabla^2\cdot\mathbf{u} + \mathbf{f}, \tag{1.6}$$

where ρ is the material density, $\mathbf{f}$ is an applied force density and λ, μ are Lamé coefficients, related to the stress tensor σ_{ij} by means of Hooks law for isotropic elastic body:

$$\sigma_{ij} = \lambda\,\mathrm{tr}(u_{ij})\delta_{ij} + 2\mu u_{ij} \tag{1.7}$$

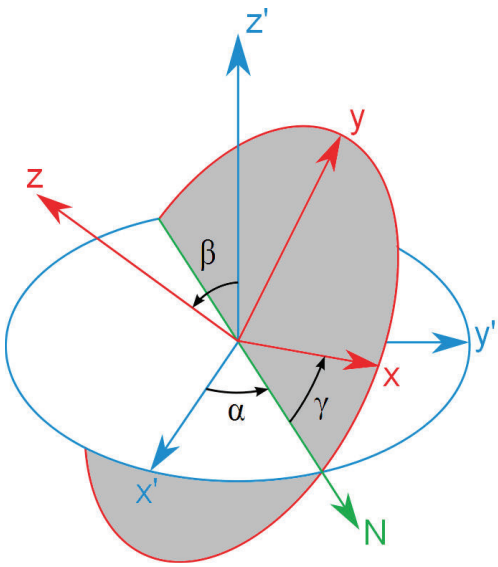

Figure 1.2**:** Euler angles transformation

where $u_{ij} = \frac{1}{2}(\partial_i u_j + \partial_j u_i)$ and δ_{ij} is the Kronecker delta. The equation (1.6) has a solution in a form of

$$\mathbf{u}(\mathbf{x}, t) = \sum_m a_m(t)\psi_m(\mathbf{x}), \tag{1.8}$$

where $\psi_m(\mathbf{x})$ is the spacial eigenfunction of the m_{th} normal mode of the sphere and $a_m(t)$ is a mode amplitude.

The eigenfunctions of an uncoupled sphere can be written in terms of the spherical harmonics:

$$\Psi_{nlm}(r, \theta, \phi) = (\alpha_{nl}(r)\hat{\mathbf{r}} + \beta_{nl}(r)R\nabla)Y_{lm}(\theta, \phi) \tag{1.9}$$

where index l is even. The radial eigenfunctions $\alpha_{nl}(r)$ and $\beta_{nl}(r)$ determine the motion in the radial and tangential directions respectively and depend on the radius R and the material of the sphere.

According to general relativity, only the five quadrupolar modes of the sphere will couple to the force density of a gravitational wave($l \equiv 2$ in the equation 1.9). For a ideal sphere all the modes are degenerate - they have the same frequency and are distinguished only by their orientation(Fig 1.3).

The gravitational force $F_m(t)$, acting on a fundamental quadrupolar mode m of the sphere from a gravitational wave is given by the overlap integral between the eigenfunctions of the sphere and the gravitational force:

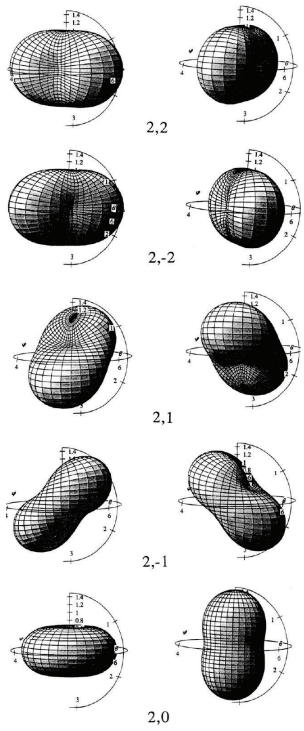

Figure 1.3**:** Visualization of the spheroidal quadrupolar modes of a sphere [25]

$$F_m(t) = \int \Psi_{2m}(x) \cdot f^{GW}(x,t) d^3x = \frac{1}{2} M \chi R \frac{\partial^2 h_m(t)}{\partial t^2} \tag{1.10}$$

Each spherical component of the gravitational field determines uniquely the effective force on the corresponding mode of the sphere. We can interpret the effective force $F_m(t)$ in each mode as the product of the physical mass of the sphere M, an effective length χR (a fraction of the sphere radius), and the gravitational acceleration $\frac{1}{2}\frac{\delta^2 h_m(t)}{\delta t^2}$. The value of the coefficient χ depends on the Poisson ratio of the sphere material. For CuAl sphere it is equal to 0.327.

1.2 Operation of a Spherical Gravitational Wave Antenna

In this section we give a description of the practical implementation of a spherical gravitational waves detector equipped with single mode capacitive resonant transducers and read-out by a low noise cryogenic amplifier (a 2-stage SQUID amplifier).

1.2.1 Secondary resonators (transducers)

As shown in the previous section, by measuring the quadrupolar modes of the sphere, we can directly measure the effective force on the sphere and thus the spherical amplitudes of the gravitational wave. To improve the displacement sensitivity, the standard technique for resonant detectors is to place secondary resonators (transducers) on their surface, strongly coupled to the quadrupolar modes.

The resonant transducer is a mechanical resonator, with a resonant frequency tuned to the one of the antenna. If both the oscillators have the same resonant frequency $\omega_s = \omega_t \equiv \omega_0$, the energy E transferred from the antenna to a transducer is given by the expression

$$E = \frac{1}{2} m_s \omega_0^2 x_a^2 = \frac{1}{2} m_t \omega_0^2 x_t^2, \tag{1.11}$$

then the displacement amplitude of the transducer is related to the sphere displacement as

$$x_t = \sqrt{\frac{m_s}{m_t}} x_a \equiv \mu^{-1} x_a, \tag{1.12}$$

so the displacement of the much lighter mass of the transducer m_t is amplified by a factor $\mu^{-1} = \sqrt{m_s/m_t}$, where m_s is the equivalent mass of the antenna. The coupled resonances split in two normal modes by $\omega_a \cdot \mu$ and their splitting increases with the transducer mass as $\sqrt{m_t}$.

Since for an ideal sphere the quadrupolar modes are degenerate, but have a different shape, we need a set of at least five transducers to be attached to the sphere in order to acquire the individual modes amplitudes.

Let's consider a sufficient set of j transducers placed on the sphere surface at arbitrary positions (ϕ_j,θ_j). For a given mode m, we can define a set of radial displacements of the sphere surface at transducer locations - a *pattern vector*. For all quadrupolar modes these vectors form an $m \times j$ *pattern matrix* $\mathbf{B}_{mj}$, defined as [20]:

$$\mathbf{B}_{mj} = \frac{1}{\alpha} \hat{\mathbf{r}} \Psi_m(\Theta_j, \phi_j) \equiv Y_m(\Theta_j, \phi_j) \tag{1.13}$$

Physically, the $\mathbf{B}_{mj}$ matrix converts the quadrupolar modes amplitudes $\mathbf{a}_m$ to the displacement amplitudes of the sphere surface at the transducers position $\mathbf{q}_j$.

Currently, in the MiniGRAIL operation we only use one-mode capacitive resonant transducers, so we are going to concentrate on them in the rest of the thesis. A model and a design considerations of two-mode inductive transducer, developed for MiniGRAIL is given in [25].

Capacitive resonant transducers

In a capacitive transducer, the constant electric field is stored in a flat capacitor, formed by the flat surface of the resonating mass and the electrode. The distance between two surfaces is of order $10-50$ micrometers. The electrode is rigidly connected

to the surface of the sphere and the resonator is tuned to the sphere modes. In principle that means that the electrode is moving together with the surface of the sphere, but since typically $\mu \sim 10^{-2}$, the motion of the electrode can be neglected. Motion of a resonating mass modulates the charge of a capacitor. The input coil of the dc-SQUID chip is coupled to the capacitive transducer via a high-Q superconductive impedance matching transformer. The matching transformer is used to match the low input impedance of the SQUID amplifier with the high impedance of the capacitor. An electromechanical scheme of one read-out channel of MiniGRAIL is shown on figure 1.4.

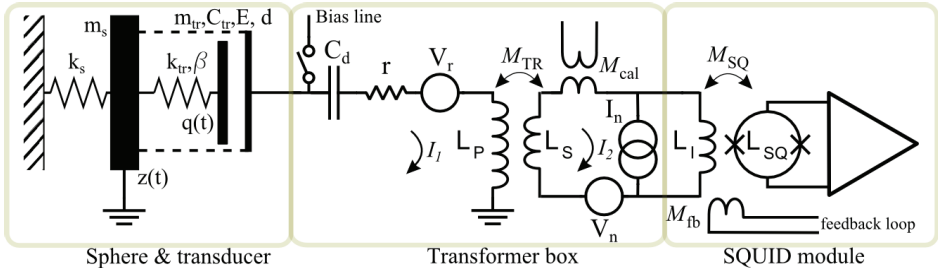

Figure 1.4**:** Scheme of MiniGRAIL read-out with a capacitive transducer coupled to a SQUID amplifier by impedance matching transformer

The mechanical part of the detector can be modeled by a set of coupled harmonic oscillators. m_s is the effective mass [1] of the sphere, m_{tr}, k_{tr}, β and are the effective mass, spring constant and damping of the transducer respectively.

Electrically, the transducer is described as a parallel plate capacitor with capacitance C_{tr} and a gap between electrodes d.
When the transducer is charged through the bias line, its motion $q(t)$ modulates the capacitor C_{tr} resulting and ac current I_1. The current couples to the SQUID input circuit through a superconducting transformer. A decoupling capacitor $C_d \gg C_{tr}$ prevents the transducer from discharging through the primary coil of the transformer.

Ideally the primary inductance of the transformer L_p should be chosen to match the impedance of the transducer and the secondary inductance L_s to match the SQUID input inductance. The mutual inductance of the transformer is given by $M = k\sqrt{L_p L_s}$, where the coupling factor $k \approx 0.85 - 0.9$.

In the scope of this chapter a SQUID is modelled as a linear current amplifier with current and voltage noise I_n and V_n respectively[26].

An electric field in the transducer gap induces a force between the capacitor plates which modifies the mechanical spring constant of the transducer resonator. For a capacitive transducer the force is attractive so the spring constant and the resonant frequency are reduced. The change of resonant frequency is an important property of a transducer, indicating how efficiently a mechanical motion of the resonator is con-

[1] Effective mass is the fraction of the physical mass of the sphere M_s, associated with each of the five quadrupolar modes and is equal to $m_s = 5/6\chi M_s$[23]

verted to an electrical signal. The electromechanical coupling coefficient β is defined as:

$$\beta = \frac{\omega_0^2 - \omega_t^2}{\omega_t^2} \tag{1.14}$$

where ω_0 is the resonant frequency when the transducer is not biased, and ω_t is the shifted frequency. For a capacitive transducer the coupling is [25]:

$$\beta = \frac{C}{d_0^2} \frac{V^2}{\omega^2 m_{eff}} \tag{1.15}$$

where C is the transducer capacitance, d_0 is the capacitor gap, V is the bias voltage and m_{eff} is the effective mass of the transducer.

By combining 1.14 and 1.15 we get:

$$f_t^2 = f_0^2 - \frac{C}{(2\pi)^2 m_{eff} d_0^2} V^2 \tag{1.16}$$

By measuring the voltage dependence of a resonant frequency of the modes we can measure the coupling of the transducer to the modes of the sphere and the effective mass, associated with the modes.

Mode Channels

In a real experiment we need to find a way to convert the measured transducer amplitudes $\mathbf{q_j}(t)$ to a spherical gravitational wave amplitude $h_m(t)$. Since the transducers are coupled to the motion of the surface of the sphere, even the single excited spherical mode would result in an excitation of most transducers. Merkowitz has shown [13] that is is possible to reconstruct each of the spherical amplitudes by building a linear combination of the measured amplitudes $\mathbf{q_j}(t)$. These linear combinations are called *mode channels* to indicate that each one corresponds to a single mode amplitude $a_m(t)$ and hence to a single amplitude $h_m(t)$. Since mode channels correspond to the quadrupolar modes of the sphere, they relate to the amplitudes $\mathbf{q_j}(t)$ by means of the pattern vector:

$$\mathbf{g_m}(t) = \mathbf{B_{mj}}^{-1} \mathbf{q_j}(t), \tag{1.17}$$

where $\mathbf{g_m}(t)$ is the mode channels vector.

Once we have built the mode channels, we can form a *detector response* matrix $\mathbf{A(t)}$ that in the absence of noise is equal to the Cartesian strain tensor $h_{ij}(t)$ in the lab frame[21]:

$$\mathbf{A} = \begin{bmatrix} g_1 - \frac{1}{\sqrt{3}} g_5 & g_2 & g_4 \\ g_2 & -g_1 - \frac{1}{\sqrt{3}} g_5 & g_3 \\ g_4 & g_3 & \frac{2}{\sqrt{3}} g_5 \end{bmatrix} \equiv \begin{bmatrix} h_{xx} & h_{xy} & h_{xz} \\ h_{yx} & h_{yy} & h_{yz} \\ h_{zx} & h_{zy} & h_{zz} \end{bmatrix} \tag{1.18}$$

According to the principal axis theorem the three eigenvectors of $\mathbf{A(t)}$ are parallel to the three principle axes of the deformation ellipsoid, and the corresponding eigenvalues show the radial deviations. To determine the direction of the incoming gravitational wave we need to know the shape and the orientation of the ellipsoid it produces. For a transverse wave, one of the eigenvalues is equal to zero, but its eigenvector will point in the direction of the incident gravitational wave. The position determination is only unique within a hemisphere - sources in opposite directions are indistinguishable.

1.2.2 Model of the sphere with capacitive transducers

Let us look at the equation of motion of a single transducer, mounted on the sphere. If we define the radial motion of the sphere at transducer position as $z(t)$ and relative distance between the resonator and the sphere surface as $q(t)$ then the inertial displacement of the resonator mass is $q + z$ and the equation of motion of the resonator is[19]

$$m_{tr}(\ddot{q}(t) + \ddot{z}(t)) + k_{tr}q(t) = f, \tag{1.19}$$

where f is the force acting between the sphere and the resonator. If we now consider a set of J transducers, and take into account that the normal mode amplitudes are related to the sphere displacement by means of the pattern matrix $\mathbf{B}_{mj}$, then for each resonator the equation of motion is:

$$m_{tr_j}\ddot{q}_j(t) + m_{tr_j}\sum_m \alpha \mathbf{B}_{mj}\ddot{a}_m(t) + k_{tr}q_j(t) = f_j. \tag{1.20}$$

The equation of motion of the sphere modes is given by[19]:

$$m_s\ddot{a}_m(t) + k_s a_m(t) = \sum_j \alpha \mathbf{B}_{mj}[k_{tr}q_j(t) - f_j(t)] + F_m(t), \tag{1.21}$$

By combining equation (1.20) and equation (1.21) we can write down the coupled equation of motion of system in a matrix form

$$\begin{aligned}\begin{bmatrix} \mathbf{m_s} & \mathbf{0} \\ \alpha\mathbf{m_{tr}}\mathbf{B}^T & \mathbf{m_{tr}} \end{bmatrix}\begin{bmatrix} \ddot{\mathbf{a}}(t) \\ \ddot{\mathbf{q}}(t) \end{bmatrix} + \begin{bmatrix} \mathbf{k_s} & -\alpha\mathbf{B}\mathbf{k_{tr}} \\ \mathbf{0} & \mathbf{k_{tr}} \end{bmatrix}\begin{bmatrix} \mathbf{a}(t) \\ \mathbf{q}(t) \end{bmatrix} \\ = \begin{bmatrix} \mathbf{I} & -\alpha\mathbf{B} \\ \mathbf{0} & \mathbf{I} \end{bmatrix}\begin{bmatrix} \mathbf{F}(t) \\ \mathbf{f}(t) \end{bmatrix},\end{aligned} \tag{1.22}$$

where $\mathbf{m_s}$, $\mathbf{k_s}$ are the diagonal matrices of effective masses and spring constants of each mode and $\mathbf{m_{tr}}$, $\mathbf{k_{tr}}$ are the diagonal matrices of masses and spring constants of each transducer.

The equation of motion does not include any deviations of quadrupole modes shape due to the attached transducers and the suspension hole. It has been shown both by finite element analysis and experimentally that for a sphere with a hole

and transducers with mass less then 1% of the sphere mass, mode shapes change is negligible. [27, 19, 12]

It is possible to simplify the equation (1.22) to $5+J$ decoupled harmonic oscillator equations by transforming it to a normal coordinate system [21]

After applying Fourier transformation we get [23]

$$[-\omega^2\mathbf{M}+\mathbf{K}]\begin{bmatrix}\mathbf{a}(\omega)\\ \mathbf{q}(\omega)\end{bmatrix}=\mathbf{A}\begin{bmatrix}\mathbf{F}(\omega)\\ \mathbf{f}(\omega)\end{bmatrix}, \tag{1.23}$$

where we have defined mass $\mathbf{M}$, elastic $\mathbf{K}$ and coupling $\mathbf{A}$ matrices

$$\begin{aligned}\mathbf{M}&\equiv\begin{bmatrix}\mathbf{m_s} & \mathbf{0}\\ \alpha\mathbf{m_{tr}}\mathbf{B}^T & \mathbf{m_{tr}}\end{bmatrix}\\ \mathbf{K}&\equiv\begin{bmatrix}\mathbf{k_s} & -\alpha\mathbf{B}\mathbf{k_{tr}}\\ \mathbf{0} & \mathbf{k_{tr}}\end{bmatrix}\\ \mathbf{A}&\equiv\begin{bmatrix}\mathbf{I} & -\alpha\mathbf{B}\\ \mathbf{0} & \mathbf{I}\end{bmatrix}\end{aligned} \tag{1.24}$$

If we also include the electric circuit, the final equation of motion of entire detector becomes [23]

$$\underbrace{\begin{bmatrix}\mathcal{M} & \mathbf{Z_{BA}} & \mathbf{0}\\ \mathbf{0}\ \mathbf{E} & \mathbf{Z} & \\ \mathbf{0}\ \mathbf{0} & & \end{bmatrix}}_{\mathcal{Z}}\begin{bmatrix}\mathbf{a}(\omega)\\ \mathbf{q}(\omega)\\ \mathbf{I_1}(\omega)\\ \mathbf{I_2}(\omega)\end{bmatrix}=\mathbf{A}'\begin{bmatrix}\mathbf{F}(\omega)\\ \mathbf{f}(\omega)\\ \mathbf{V_r}(\omega)\\ \mathbf{V_n}(\omega)\end{bmatrix}, \tag{1.25}$$

where $\mathcal{M}=-\omega^2\mathbf{M}+\mathbf{K}$, $\mathbf{E}$ is a diagonal matrix of electric fields in transducers gap, $\mathbf{Z}$ is the $2J\times 2J$ impedance matrix, defined as

$$\mathbf{Z}=\begin{bmatrix}\mathbf{Z_{11}} & \mathbf{Z_{12}}\\ \mathbf{Z_{21}} & \mathbf{Z_{22}}\end{bmatrix},$$

where each component $\mathbf{Z_{ij}}$ is a diagonal matrix of $J\times J$ elements with diagonal components equal to

$$\begin{aligned}\mathbf{Z}^j_{\mathbf{11}}&=r^j+i\omega L^j_p+\frac{1}{i\omega C^j_{tr}},\\ \mathbf{Z}^j_{\mathbf{12}}&=-i\omega M^j_{TR},\\ \mathbf{Z}^j_{\mathbf{21}}&=-i\omega M^j_{TR},\\ \mathbf{Z}^j_{\mathbf{22}}&=i\omega({L_s}^j+{L_I}^j).\end{aligned} \tag{1.27}$$

$\mathbf{Z_{BA}} = \begin{bmatrix} -\alpha\mathbf{B} \\ \mathbf{I} \end{bmatrix} \frac{\mathbf{E}}{i\omega}$ is the $(5+J)\times J$ back action matrix, which represents the effect of the current I_p on the mechanical system, and $\mathbf{A}' = \begin{bmatrix} \mathbf{A} & \mathbf{0} \\ \mathbf{0} & \mathbf{I} \end{bmatrix}$

We can invert the $\mathcal{Z}$ matrix and rewrite the equation (1.25) in the form

$$\begin{bmatrix} \mathbf{a}(\omega) \\ \mathbf{q}(\omega) \\ \mathbf{I_1}(\omega) \\ \mathbf{I_2}(\omega) \end{bmatrix} = \mathcal{Z}^{-1}\mathbf{A}' \begin{bmatrix} \mathbf{F}(\omega) \\ \mathbf{f}(\omega) \\ \mathbf{V_r}(\omega) \\ \mathbf{V_n}(\omega) \end{bmatrix} \equiv \mathbf{G} \begin{bmatrix} \mathbf{F}(\omega) \\ \mathbf{f}(\omega) \\ \mathbf{V_r}(\omega) \\ \mathbf{V_n}(\omega) \end{bmatrix}. \tag{1.28}$$

Equation (1.28) gives us the relation between the forces generated in the system and the amplitudes of the sphere modes, transducers displacements and the currents in the electrical read-out circuits. In practice the only values we can measure experimentally are the currents in the input coils of the SQUIDs $\mathbf{I_2}$, so we are only interested in J last rows of $\mathbf{G}$ matrix, denoted by $\mathbf{G_I}$. The current at the SQUID input also includes the contribution of the current noise from the SQUID itself:

$$\mathbf{I}(\omega) = \mathbf{G_I} \begin{bmatrix} \mathbf{F}(\omega) \\ \mathbf{f}(\omega) \\ \mathbf{V_r}(\omega) \\ \mathbf{V_n}(\omega) \end{bmatrix} + \mathbf{I_n}(\omega) \equiv \mathbf{G_I}\mathcal{F}(\omega) + \mathbf{I_n}(\omega) \tag{1.29}$$

We can compute a noise spectral density matrix $\mathbf{S_I}$ defined as

$$\mathbf{S_I} = \mathbf{I}(\omega)\mathbf{I}^*(\omega) = \mathbf{G_I}\mathcal{F}\mathcal{F}^*\mathbf{G_I^*} + \mathbf{G_I}\mathcal{F}\mathbf{I_n^*} + \mathbf{I_n}\mathcal{F}^*\mathbf{G_I^*} + \mathbf{I_n}\mathbf{I_n^*} \tag{1.30}$$

The SQUID noise is not correlated with other noise sources in the system, so the terms $\mathbf{F}\mathbf{I_n^*}$ and $\mathbf{I_n}\mathbf{F}^*$ cancel out, moreover the the noises of different SQUIDs are also uncorrelated, so $\mathbf{I_n}\mathbf{I_n^*}$ contains only autocorrelation terms, or in other words the matrix $\mathbf{S_{I_n}} = \mathbf{I_n}\mathbf{I_n^*}$ is diagonal. As a result the noise spectral density matrix in the equation (1.30) is reduced to

$$\mathbf{S_I} = \mathbf{G_I}\mathcal{F}\mathcal{F}^*\mathbf{G_I}^* + \mathbf{S_{I_n}} \tag{1.31}$$

Generally, a transducer does not couple only to a single sphere mode, but to a set of modes. This means that different transducers couple through the sphere modes and the noise spectra of transducers are correlated, so $\mathbf{S_I}$ matrix is not diagonal. Further we will discuss a way to combine the transducer outputs to build the uncorrelated channels.

We limit the analysis to the case where in the absence of gravitational waves signal the forces generated in the system are due to the thermal noise. The noise spectral density of a mechanical oscillators is given by [28]

$$\begin{aligned} S_F &= 4k_BT\frac{m_s\omega_s}{Q_s} \\ S_f &= 4k_BT\frac{m_{tr}\omega_{tr}}{Q_{tr}} \end{aligned} \tag{1.32}$$

Electric noise due to the losses in the capacitor, denoted by r, is

$$S_{V_r} = 4k_B T r \tag{1.33}$$

Voltage and current noises of the SQUID amplifier, according to Clarke-Teshe model [26], are

$$\begin{aligned} S_{V_n} &= 11\frac{k_B T}{R_s} M_{SQ}^2 \omega^2 \\ S_{I_n} &= 16\left(\frac{L_{SQ}}{M_{SQ}}\right)^2 \frac{k_B T}{R_s}, \end{aligned} \tag{1.34}$$

where R_s is the shunt resistance of the SQUID.

1.2.3 Detector sensitivity

Strain sensitivity

The performance of a gravitational waves detector is characterised by the ratio of the output signal due to the gravitational waves to the one due to intrinsic noise of the detector.

We can write down the equation (1.10) in a frequency domain [20]

$$\mathbf{F}^{GW} = -\frac{1}{2} M\chi R\omega^2 \mathbf{h_m} = -\frac{1}{2} M\chi R\omega^2 \mathbf{T_V} \begin{pmatrix} h_+ \\ h_\times \end{pmatrix}, \tag{1.35}$$

then in the absence of noise the output signal of the detector is

$$\mathbf{I}^{GW}(\omega) \equiv \mathbf{G_I} \begin{bmatrix} \mathbf{F}^{GW}(\omega) \\ \mathbf{0} \\ \mathbf{0} \\ \mathbf{0} \end{bmatrix} = \hat{\mathbf{G}}_\mathbf{I} \mathbf{F}^{GW}(\omega) = -\frac{1}{2} M\chi R\omega^2 \hat{\mathbf{G}}_\mathbf{I} \mathbf{T_V} \begin{pmatrix} h_+ \\ h_\times \end{pmatrix}, \tag{1.36}$$

where $\hat{\mathbf{G}}_\mathbf{I}$ is a submatrix of $\mathbf{G_I}$ containing only the first row of 5 elements.
In the presence of noise the signal-to-noise ratio for a gravitational wave signal of amplitude $\mathbf{h} = \begin{pmatrix} h_+ \\ h_\times \end{pmatrix}$ is given by [29]

$$SNR^2 = \int_{-\infty}^{\infty} \sigma(w) \frac{d\omega}{2\pi}, \tag{1.37}$$

where the integrand

$$\sigma(\omega) = \mathbf{I}^{*GW}(\omega) \mathbf{S_I}^{-1} \mathbf{I}^{GW}(\omega) = \frac{(M\chi R)^2 \omega^4}{4} \mathbf{h}^* \mathbf{T}_\mathbf{V}^* \hat{\mathbf{G}}_\mathbf{I}^* \mathbf{S_I}^{-1} \hat{\mathbf{G}}_\mathbf{I} \mathbf{T_V} \mathbf{h}, \tag{1.38}$$

gives the available SNR power density per unit bandwidth.

At a sensitivity limit $SNR = 1$ and since we have no information about the polarization of the incident wave we can set $h_\times \equiv 0$, $h_+ \equiv h$, so $\mathbf{h}^*\mathbf{h} = h^2$. We can now solve the equation (1.38) for h

$$h(\omega) = \left(\frac{4}{(M\chi R)^2 \omega^4} \frac{\mathbf{S_I}}{\mathbf{T_V^* \hat{G}_I^* \hat{G}_I T_V}} \right)^{1/2} \equiv \left(\frac{4}{(M\chi R)^2 \omega^4} \frac{\mathbf{S_I}}{\mathbf{Tf}} \right)^{1/2}, \tag{1.39}$$

where $\mathbf{Tf} = \mathbf{T_V^* \hat{G}_I^* \hat{G}_I T_V}$ is the transfer matrix between the gravitational wave force and the current spectral density at the input of the SQUIDs. Note that the transfer matrix includes an angular dependent $\mathbf{T_V}$ component and thus is direction dependent. By averaging over all directions we get the expression for the average sky sensitivity of the detector [28]

$$\langle h(\omega) \rangle = \frac{2\sqrt{5}}{M\chi R\omega^2 \sqrt{\mathrm{trace}(\mathbf{\hat{G}_I^* S_I^{-1} \hat{G}_I})}}. \tag{1.40}$$

The amplitude of a gravitational wave, resulting in a $SNR = 1$ is called the strain sensitivity and is conventionally referred to as $S_{hh}(\omega) \equiv h(\omega)^2$.

Directional sensitivity

From the equations in the previous chapter we can conclude that in the absence of noise the spherical detector is able to locate the exact direction of the gravitational waves source. If the noise contribution is not negligible, the angular resolution is degraded. We define the angular resolution as

$$\Delta\Omega = \pi((\theta - \theta_0)^2 + \sin^2\theta_0(\phi - \phi_0)^2), \tag{1.41}$$

where (ϕ_0, θ_0) is the actual direction of the source and (ϕ, θ) is the calculated direction. Physically, $\Delta\Omega$ is the area of a circle on the unit sphere with a center at (ϕ_0, θ_0) and a radius showing the difference between a real and a calculated direction. It can be shown [30] that $\Delta\Omega$ depends on the SNR as

$$\Delta\Omega = \frac{2\pi}{SNR}. \tag{1.42}$$

A result of 200 Monte Carlo simulations for different signal-to-noise ratios reported in [30] is shown on figure 1.5. The simulated signal was a linearly polarised gravitational wave propagating in the direction $\phi_0 = 2\,rad$, $\theta_0 = 1\,rad$. For $SNR = 1$ the points are distributed almost uniformly over the sky, and the direction estimation is not possible. For the $SNR = 10$, the distribution of trials starts to converge on the vicinity of the true wave direction. From these simulations the minimum SNR required for direction reconstruction is approximately 10 for a spherical detector.

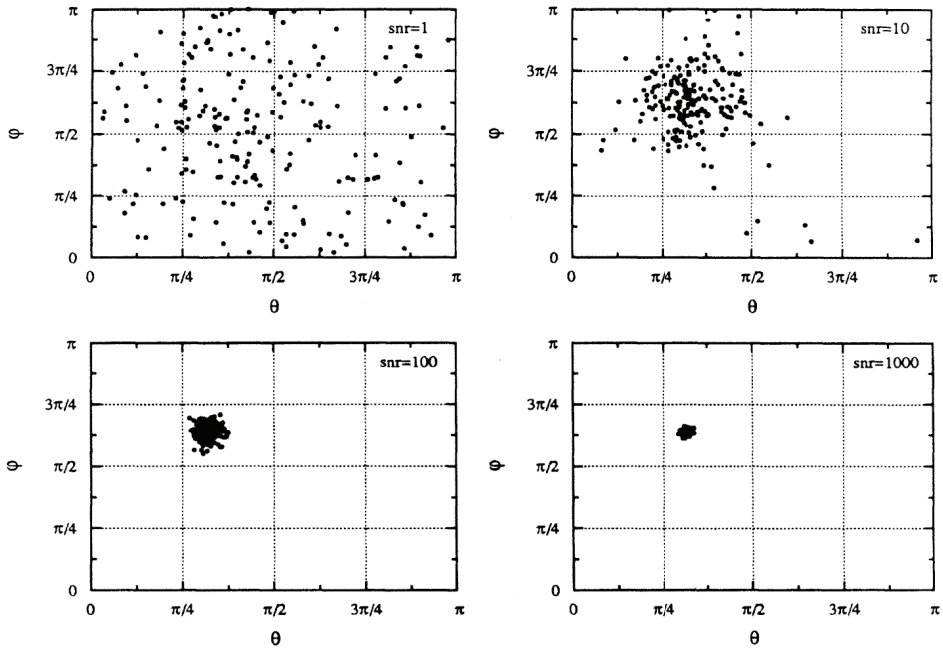

Figure 1.5**:** Calculated wave direction for 200 simulations each for various values of the signal- to-noise ratio. The simulated wave signal was a linearly polarised gravitational wave propagating in the direction $\phi_0 = 2\,rad$, $\theta_0 = 1\,rad$. Figure is taken from [30]

1.2.4 Measuring strain sensitivity of a real detector

In a real experiment the signal we are measuring is a voltage at the output of the SQUID electronics. The voltage can easily be converted to the current at the input of the SQUIDs $\mathbf{I}(\omega)$ and if we preserved the phase information we can build the noise spectral density matrix $\mathbf{S_I}$ from equation (1.30). In order to calculate the sensitivity we also need to evaluate the transfer matrix $\mathbf{Tf}$. It can either be calculated analytically, as described in [31, 32], or measured experimentally as we do in this work. The main disadvantage of the calculated transfer matrix, besides the system's complexity, is that we need to model the real system as precisely as possible, otherwise the inconsistency between the transfer matrix and the measured noise spectra would produce artifacts on a strain sensitivity curve. Purely theoretical works, as the ones listed above, obviously do not have this problem, as they use the same set of system parameters to generate the noisy detector output and to build the transfer matrix.

In particular, we only have to measure the admittance submatrix $\hat{\mathbf{G}}_\mathbf{I}$ as $\mathbf{T_V}$ is a purely geometric factor depending on the detector's reference frame orientation. From the equation (1.36) we see that if we can find the way to apply a known force to the normal modes of the sphere and measure the output current we can easily build

the $\hat{\mathbf{G}}_\mathbf{I}$ matrix. A force applied to the surface of the sphere excites a combination of the normal modes, defined by the pattern vector. For a set of calibrators, radially exciting the sphere, the forces, acting on the modes are

$$\mathbf{F_m}(\omega) = \alpha \mathbf{B_c} \mathbf{F_c}(\omega), \tag{1.43}$$

where $\mathbf{B_c}$ is the pattern matrix for calibrators positions and $\mathbf{F_c}$ are the forces applied to the sphere surface by calibrators. By generating a proper linear combination of calibrators forces we can simulate the effect of gravitational wave coming from any direction. We suggest using a set of at least 5 mass-loaded PZT calibrators, as they are very compact and give more flexibility than a single detuned capacitive calibrator used in the previous runs [25]. In chapter 4 we will also discuss the way of measuring the force that calibrators apply to the sphere.

It is convenient to convert the current at transducers output into 5 equivalent mode channel currents, as they correspond to spherical components of the gravitational wave as described in section 1.2.1. The mode channel current vector construction is straightforward

$$\mathbf{I_m}(\omega) = \mathbf{B}\mathbf{I}(\omega) = \alpha \mathbf{B} \hat{\mathbf{G}}_\mathbf{I} \mathbf{B_c} \mathbf{F_c}(\omega). \tag{1.44}$$

Because the mode channels are statistically independent, their current spectral density matrix $\mathbf{S_{I_m}}(\omega) = \mathbf{I_m}(\omega)\mathbf{I_m^*}(\omega)$ is diagonal and we can treat a 5-channel spherical detector as a set of 5 independent single-channel detectors, applying much simpler data analysis and filtering algorithms developed for the bars.

From equation (1.44) we see that in order to calculate the $\hat{\mathbf{G}}_\mathbf{I}$ matrix from known $\mathbf{F_c}(\omega)$ and measured $\mathbf{I}(\omega)$ we need to invert the pattern matrix $\mathbf{B}$. The solution of the problem depends on the number and the position of transducers. If we have less than five transducers - the system is underdetermined, and the mode channels cannot be built.

Since five quadrupolar modes of the sphere contain complete information about the spherical amplitudes of a gravitational wave, it would be natural choice to try the configuration with 5 transducers tuned to the sphere modes. However Johnson and Merkowitz have discovered that for every arrangement of five transducers they tried the transducer-mode coupling was always non optimal [20]. They achieved the best results with a special 6-transducer arrangement called *Truncated Icosahedral Gravitational Wave Antenna* (TIGA).

Special transducers arrangement - TIGA

TIGA consists of a set of six transducers placed on pentagonal faces of a Truncated Icosahedron (TI). The resonators arrangement for TIGA is shown on figure 1.6. The transducers are placed at two polar angles, $\theta = 37.3773^o$ and 79.1876^o. Their azimuthal angles are multiple of 60^o.

The high symmetry of the TI arrangement affects its pattern matrix. Each pattern vector is orthogonal to the others and has the same magnitude $\sqrt{\frac{3}{2\pi}}$:

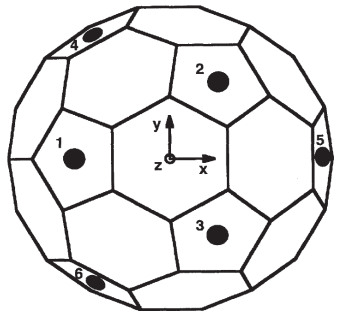

Figure 1.6**:** The truncated icosahedral gravitational wave antenna (TIGA) with secondary resonator locations indicated. The numbering of the transducers positions corresponds to the ordering used in the rest of this thesis. Figure is taken from [19].

$$\mathbf{B}\mathbf{B}^* = \frac{3}{2\pi}\mathbf{I}, \tag{1.45}$$

where $\mathbf{I}$ is the 5×5 identity matrix. This property means that the pattern matrix for TIGA transducer arrangement is a unitary matrix, and we can substitute the inversion, which is not possible for rectangular 5×6 $\mathbf{B}$ matrix, with a transpose. It also shows that there is indeed no cross-correlation between the modes and the sphere modes are a direct measurement of the gravitational spherical amplitudes.

In addition to orthogonality, the sum of the components of each pattern vector is zero.

$$\mathbf{B1} = \mathbf{0}, \tag{1.46}$$

where $\mathbf{1}$ is a 6×1 column vector of ones and $\mathbf{0}$ is a 5×1 column vector of zeroes.

A practical advantage of the TIGA configuration is that it only involves the use of equal mass radial transducers similar to the ones developed for other resonant detectors.

A disadvantage of the TIGA configuration is that we use 6 transducers outputs to reconstruct 5 mode channels, so the system is overdetermined. In case of a real detector in the presence of significant noise and system asymmetry the reconstruction of mode channels is not trivial.

Another approach to B matrix reversal

In this work we use another way of inverting the pattern matrix, that does not involve relying on any particular transducer placement symmetry. The same approach is used when building a numerical model of the sphere in [32]. Besides the 5 quadrupole modes, coupled to the gravitational waves, we also include a monopole mode, so the equation (1.13) becomes

$$\mathbf{B}_{mj} = Y_{1..5}(\theta_j, \phi_j) + \frac{\mathbf{I}_6}{\sqrt{4\pi}}. \tag{1.47}$$

We have included a 6-th column to the matrix $\mathbf{B}$ so it becomes 6×6 invertible matrix. In principle, we could have included any of the sphere modes into the analysis, but the advantage of the monopole mode is that it is orthogonal to the quadrupole modes, so the mode channels are still uncorrelated. The frequency of the monopole mode is roughly twice the frequency of the first quadrupole modes, so its coupling to the transducers is very weak. But it does not matter since we do not actually use the monopole mode in the detector's data analysis, as it is only included to make the pattern matrix invertible and is excluded in the further calculations. However, it can be potentially used to test the alternative theories of gravity [22].

Noise temperature of the detector

The performance of resonant gravitational wave detectors is often compared by their sensitivity to the burst gravitational wave signal. For a given strain amplitude of a gravitational wave $h(\omega)$, the energy deposited to the resonator is [23]

$$E^{GW} = \frac{c^3}{16\pi G}\omega^2 |h(\omega)|^2 \Sigma, \tag{1.48}$$

where G is the gravitational constant, c is the speed of light and Σ is the energy cross section of the detector Σ given by

$$\Sigma = \frac{G\rho V_S^5}{c^3 f_0^3}\Pi, \tag{1.49}$$

where , ρ and V_S^5 are the density and the sound velocity of the detector material. Π is the reduced energy cross section which depends on the geometry of the detector and the Poisson ratio of its material. For MiniGRAIL $\Pi = 0.215$.

If E^{GW} is the energy deposited by gravitational wave, then we can express the signal-to-noise ratio of a single-channel detector as [30]

$$SNR = \frac{E^{GW}}{k_B T_n}, \tag{1.50}$$

where T_n is the detector noise temperature for pulse detection. A spherical detector has five independent mode channels and the total SNR of a spherical detector is a sum of the SNR of the mode channels

$$SNR = \sum_{m=1}^{5} SNR_m = \frac{E_{tot}^{GW}}{k_B T_n}, \tag{1.51}$$

where E_{GW}^{tot} is the total energy deposited in the sphere. Here we assume that he noise temperature of the mode channels is equal.

It can be shown that for the same noise temperature the spherical detector has a sky averaged signal-to-noise ratio about 40-50 times higher than a bar of equivalent size [30, 13].

Simulated sphere response to calibration excitation

An experimental way of measuring a transfer function in section 1.2.4 relies on the assumption that the real sphere behaviour is the same as the one of an ideal sphere and we can use the spherical harmonics model described in section 1.1.2. A good way to test the validity of the model is to try to solve the inverse problem of direction reconstruction.

Since there are no known sources of gravitational waves, we have to use the calibrators to excite the sphere. Once again, we can convert the signal from the transducers to the mode channels and build the response matrix $\mathbf{A}$. To estimate the direction of the excitation we calculate the eigenvectors and eigenvalues of $\mathbf{A}$. Depending on the number of calibrators installed we can either use a set of calibrators to simulate the gravitational wave excitation or use a single calibrator to apply a radial impulse excitation on the surface of the antenna.

The major difference of the impulse excitation from a gravitational wave excitation is the shape of the deformation ellipsoid.

The calibration impulse will excite the set of a spherical harmonics defined by a pattern vector at the calibrator's position

$$\mathbf{a} \propto \mathbf{Y}(\phi_c, \theta_c)\mathbf{F_c}, \tag{1.52}$$

where $\mathbf{F_c}$ is the force that calibrator applies on the surface of the sphere. The "calibration" deformation ellipsoid has maximum radial deviation at the location of the impulse, and two radial deviations in the orthogonal directions having opposite sign and half amplitude. Therefore, the location of the impulse is given by the eigenvector with the largest eigenvalue.

For the gravitational wave coming from the same direction the amplitudes of the spherical harmonics are related to the gravitational wave strain amplitudes by means of $\mathbf{T_V}$ matrix

$$\mathbf{a} \propto \mathbf{h_m} \propto \mathbf{T_V} \begin{pmatrix} h_+ \\ h_\times \end{pmatrix} \tag{1.53}$$

Since gravitational wave strain field is orthogonal to the propagation direction, the resulting deformation ellipsoid will have a zero amplitude in the wave direction and equal nonzero amplitudes in the orthogonal directions.

We have performed the tests both on a simulated and on the real MiniGRAIL sphere. To see if the suspension influences the shape of the quadrupolar modes, we have simulated the behaviour of both ideal and suspended spheres. First we have performed the simulation by Finite Element Analysis (FEA) software Pro/ENGINEER Mechanica [33]. The elastic properties of the sphere were set to match the properties of $CuAl6\%$ alloy.

As we already mentioned in section 1.1.2 the quadrupolar modes of an ideal sphere are degenerate. This is also true for simulation of an ideal sphere, but for a sphere with a hole they are not degenerate, but are grouped in into two doublets and a singlet. First doublet ($2973.58\,Hz$, $2973.71\,Hz$) corresponds to modes Y_1, Y_2, second ($2990.77\,Hz$, $2990.85\,Hz$) to Y_3, Y_4 and the singlet ($3006.00\,Hz$) corresponds to Y_5 mode. This results agree very well with the results obtained on a real TIGA prototype [19].

In the simulation we did a series of tests where we applied the radial force at different points of the sphere surface and recorded the surface displacement at transducers position. First two tests were made on a model of an ideal sphere with TIGA and MiniGRAIL (see section 1.3.2) transducers layout. The third test was performed on a suspended sphere with TIGA transducers arrangement.

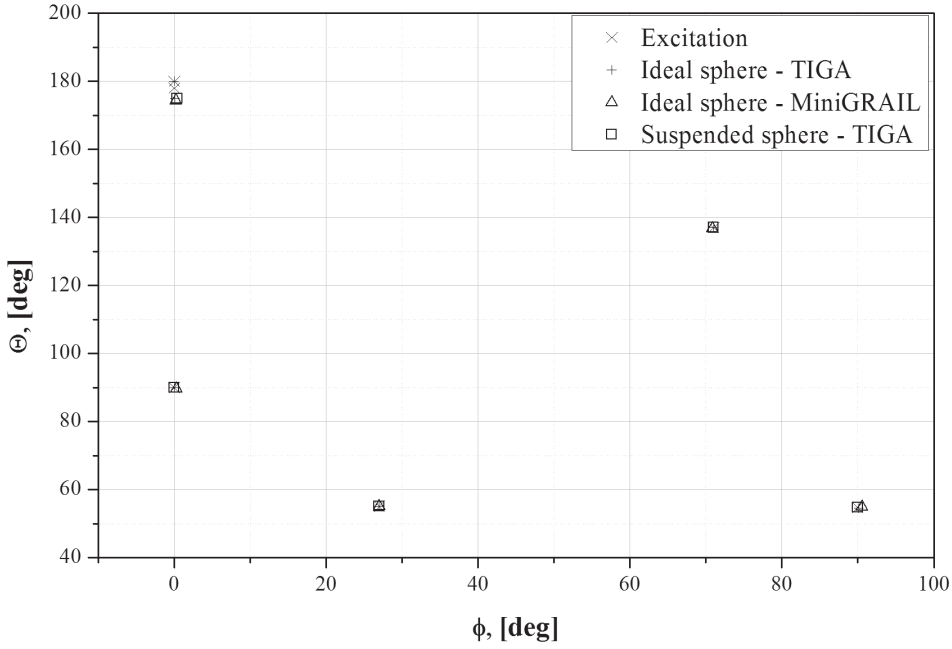

Figure 1.7**:** Calculated locations of the excitation points for an ideal sphere and a sphere with the suspension hole.

Recorded time series were further processed with Matlab [34] scripts. For inversion of the pattern matrix in TIGA arrangement we used the corresponding model described in section 1.2.4. For MiniGRAIL layout we used an approach from section 1.2.4

From equation (1.4) we can see that some spherical harmonics might have a zero amplitude for a particular excitation direction. For instance, the excitation from the top of the sphere ($\phi = 0^o$, $\theta = 180^o$) will only excite Y_5 mode. We have performed

	Excitation		Ideal sphere TIGA		Ideal sphere MiniGRAIL		Suspended sphere TIGA	
#	ϕ	θ	ϕ	θ	ϕ	θ	ϕ	θ
1	0	180	0	179,9658	0	179.9573	-	-
2	0	90	0,0342	89,9306	0,0221	89,9687	0,318	89,6016
3	90	54,74	90,1441	54,5145	90,0095	54,7612	90,564	54,8575
4	0	178	0,1188	175,001	0,4401	174,9991	0,2395	174,3737
5	27	55	26,9986	55,0003	26,998	54,9991	27,0093	55,0869
6	71	137	70,9883	137,0039	70,9907	137,0021	70,8528	136,7879

Table 1.1**:** Calculated locations of the excitation points for an ideal sphere and a sphere with the suspension hole.

a simulation for a total of 6 points, with 4 of them only exciting only a subset of 5 quadrupolar modes and 2 arbitrary points exciting all the modes. The result of the direction reconstruction for 6 excitation points is shown on figure 1.7 and table 1.1.

The expected and calculated values of the spherical harmonics amplitudes are shown in table 1.2. The amplitudes of the modes are normalized so that the highest amplitude is set to 1.

As we can see from the simulations, the direction reconstruction algorithms, that rely on the model of the ideal sphere are also working perfectly for the suspended sphere. As for the real MiniGRAIL setup we have discovered that its behaviour is substantially different from the theoretical model. However with some modifications we were able to calculate the direction of the calibration pulse. We will discuss the results in the chapter 4.

1.3 MiniGRAIL

In the rest of this chapter we will focus on the actual design of the MiniGRAIL detector.

From equation (1.49) we see that the energy cross section of the detector is proportional to ρV_S^5, so it can be improved by using high-density, high-sound-velocity materials. After considering many possibilities [35] we have chosen a $CuAl6\%$ alloy because of its high mechanical quality factor ($Q \sim 10^7$ at low temperature) and a high sound velocity ($V_S \simeq 4100$ m/s). Unlike aluminium alloys which yield even higher Q, $CuAl$ does not become superconducting and demonstrates a good thermal conductivity at low temperature, allowing to cool a sphere below 100 mK [36]. It is also not toxic like Be alloys.

The sphere has a diameter of 68 cm, a mass of about 1.4 ton and the frequencies of spheroidal quadrupolar modes around 2980 Hz at 4.2 K. The general scheme of a MiniGRAIL setup is shown on figure 1.8.

The goal of the project is to operate MiniGRAIL at a thermodynamic temperature of 20 mK, equipped with six transducers coupled to nearly quantum limited double-

	Y1	Y2	Y3	Y4	Y5
1. $\phi = 0$, $\theta = 180$					
a.	0	0	0	0	1
b.	2.0E-4	-6.0E-4	-5.0E-4	9.0E-4	1
c.	1.0E-4	4.0E-4	1.3E-3	3.0E-4	1
d.	–	–	–	–	–
2. $\phi = 0$, $\theta = 90$					
a.	1	0	0	0	$-\frac{1}{\sqrt{3}} \approx -0.5774$
b.	1	0.0012	-0.0038	-0.0024	-0.5774
c.	1	0.0008	0.0032	0.0011	-0.5774
d.	1	0.0111	4.0E-4	0.014	-0.5833
3. $\phi = 90$, $\theta = 54.7356$					
a.	$-\frac{1}{\sqrt{2}} \approx -0.7071$	0	1	0	0
b.	-0.7065	-2.4E-3	1	-4.1E-3	9.7E-3
c.	-0.7069	-1.0E-3	1	1.0E-3	-1.3E-3
d.	-0.7126	-1.2E-2	1	-1.3E-3	-2.3E-3
4. $\phi = 0$, $\theta = 178$					
a.	1.1E-3	0	0	-0.0605	1
b.	6.7E-3	1.3E-3	-2.0E-4	-0.1521	1
c.	6.6E-3	5.0E-4	1.2E-3	-0.1521	1
d.	2.6E-2	1.0E-3	-6.0E-4	-0.1697	1
5. $\phi = 27$, $\theta = 55$					
a.	0.4711	0.6484	0.5095	1	-0.009
b.	0.4711	0.6483	0.5095	1	-0.009
c.	0.4711	0.6482	0.5095	1	-0.009
d.	0.4757	0.6510	0.5137	1	-0.011
6. $\phi = 71$, $\theta = 137$					
a.	-0.3886	0.3036	-1	-0.3443	0.3701
b.	-0.3884	0.3037	-1	-0.3445	0.3702
c.	-0.3884	0.3037	-1	-0.3445	0.3702
d.	-0.3940	0.3102	-1	-0.3479	0.3659

Table 1.2**:** Spherical harmonics amplitudes. a - calculated form the elastic model of an ideal sphere, b,c - from FEA of ideal sphere, d - from FEA of the sphere with hole

stage SQUID amplifiers [37].

1.3.1 Mechanical vibration insulation system and cryogenics

The sphere is suspended from the center with a 20 mm gold-plated copper rod. The rod is connected to the last mass of the mechanical vibration isolation system which consists of seven mass-spring stages suspended from the top of the Dewar. The first four masses are made of $CuAl6\%$ hanging from three steel ring springs. The lower three masses are made of copper, and are connected with gold-plated copper rods. Each stage acts as a mechanical low pass filter with cut-off frequency around 120 Hz and a resulting attenuation at the resonance frequency of the sphere of about 50 dB

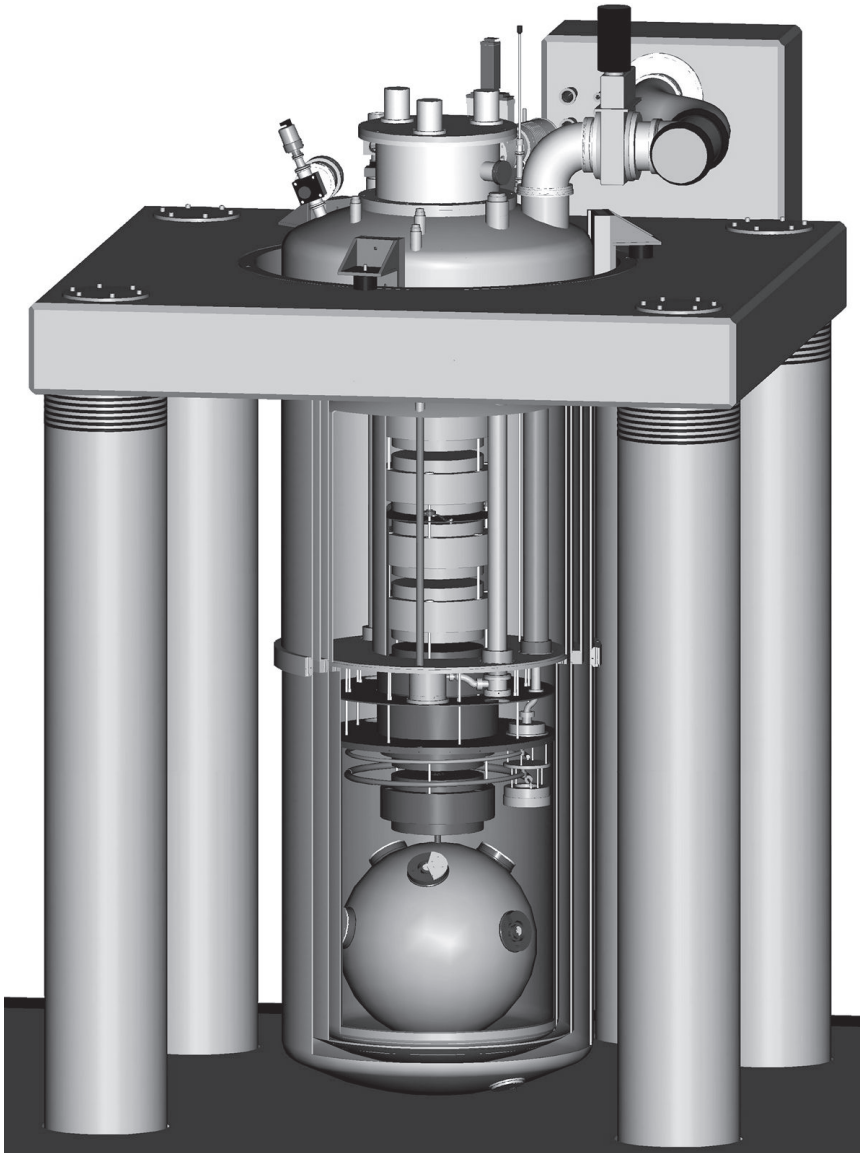

Figure 1.8**:** Schematic picture of the MiniGRAIL set up. The sphere is suspended from a vibration insulation stack consisting of a seven mass-spring stages. A dilution refrigerator is installed for cooling the sphere to cryogenic temperatures. Six resonant transducers are placed on the sphere.

per stage [38], [39]. The overall attenuation is estimated to be over 350 dB.

The sphere with the vibration insulation system is suspended in vacuum inside the cryogenic Dewar. 340 L liquid helium and 200 L nitrogen baths are located in the upper part of a Dewar. The lower part has no cryogenic liquids, and contains radiation shields, attached to nitrogen, helium baths and to Still and 50 mK plates. The Dewar is installed on a platform placed on a concrete island which is mechanically decoupled from the laboratory building.

A dilution refrigerator is used to cool the sphere below 4.2 K. The last three copper masses are thermally coupled to a mixing chamber. Is is naturally very important to have a very good thermal link between the mixing chamber and the sphere in order to reach the lowest temperatures. On the other hand is is also important to maintain a low mechanical coupling, so that the low thermal noise of the sphere would not be spoiled by the mechanical vibrations coming from the dilution refrigerator. We have made a very soft annealed copper "Jellyfish" link(see figure 1.9(b)), that connects the mixing chamber to a suspension mass 5. Three stages of suspension and a soft thermal link effectively decouple the sphere from vibrations of the dilution refrigerator.

The two upper CuAl masses 4 and 3 are coupled to 50 mK and Still plates respectively by means of the similar soft thermal links.

During the previous runs the minimal reached temperature of the sphere was 67 mK with a temperature gradient between the mixing chamber and the sphere of about 20 mK. With a new, more powerful dilution refrigerator unit installed recently we expect reaching even lower temperatures.

1.3.2 Transducers

The picture of the MiniGRAIL sphere with transducers and calibrators mounted are shown on figure 1.10. Because of the limited spacing inside the Dewar the three lowest transducers were placed at polar angle of 67.8^o - higher than TIGA's 79.1876^o. the upper transducers are placed at a proper TIGA angle of $\theta = 37.3773^o$. The azimuthal angles are the ones of TIGA arrangement. The difference in the inclination angle is certainly above the tolerance of a TIGA model [21], so in all future calculations we will use a 6×6 pattern matrix with included monopole mode. We have also placed 6 mass-loaded PZT calibrators at the same θ angles as transducers but shifted by 60^o in azimuthal angles. The seventh calibrator is placed at an arbitrarily selected position of $\phi = 33^o$, $\theta = 51^o$ and is used to test the direction reconstruction algorithms. The shiny cylindrical boxes attached to the last suspension mass are housings for the superconducting transformers and SQUID modules. They are made from led-plated copper and covered with cryoperm foil for electromagnetic protection.

1.3.3 Strain Sensitivity

MiniGRAIL strain sensitivity measured with one transducer during run 6 (first sensitivity run) is shown on figure 1.11. The transducer was charged to 200 Volt and the sphere thermodynamic temperature was about 5 K.

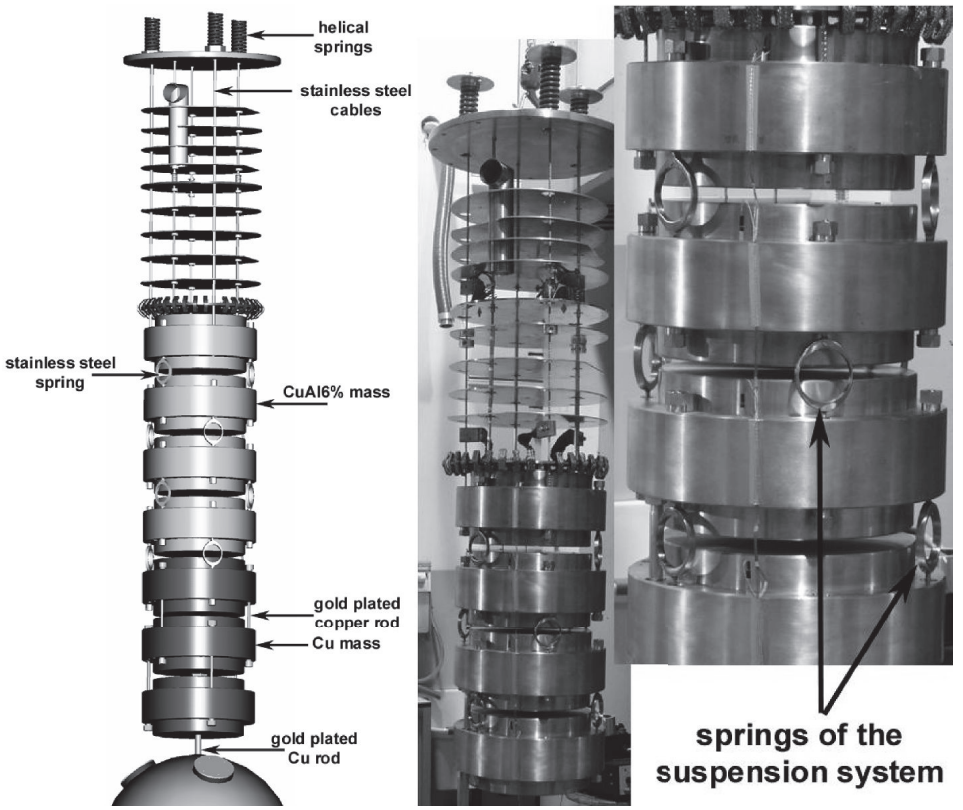

(a)

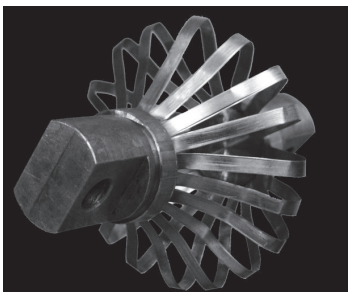

(b)

Figure 1.9**:** (a) - MiniGRAIL vibration insulation system.(b)- a soft "Jelly-fish" link used to thermally couple the sphere to the dilution refrigerator.

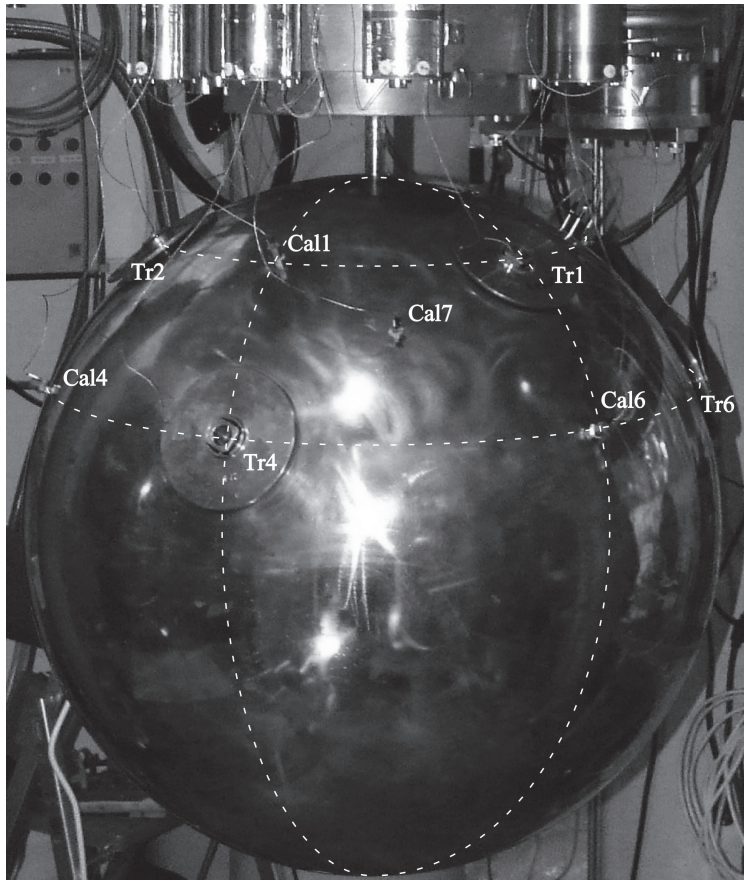

Figure 1.10**:** MiniGRAIL sphere with all transducers and calibrators installed. Transducers are placed in TIGA configuration and 6 calibrators are are placed at the same polar angles as transducers but shifted by 60^o in azimuthal angles. Calibrator 7 is installed at ($\phi = 33^o$, $\theta = 51^o$)

We reached a peak strain sensitivity of $(1.5 \pm 0.6) \cdot 10^{-20} Hz^{-1/2}$ at $2942.9\,Hz$ and a strain sensitivity of about $5 \cdot 10^{-20} Hz^{-1/2}$ over a bandwidth of $30\,Hz$. This correspond to a strain amplitude of $h \simeq 2.5 \cdot 10^{-18}$ at $3\,kHz$ for a burst signal of $1\,ms$ [12]. For a sphere of $68\,cm$ in diameter like the one of MiniGRAIL, it is equivalent to a displacement sensitivity, at $3\,kHz$, of $1.6 \cdot 10^{-19}\,m$. From equation (1.50) we estimate that the detector is sensitive to a burst signal with an impulse energy of about $T_N \sim 50\,mK$. This sensitivity would be enough to detect supernova explosions in our galaxy. The expected event rate, however, is only a few per century. To increase the event rate to at least several per year, it is necessary to improve the sensitivity to $S_{hh_{min}} \leq 10^{21}$ and reach the Virgo cluster of galaxies, which is at a distance of

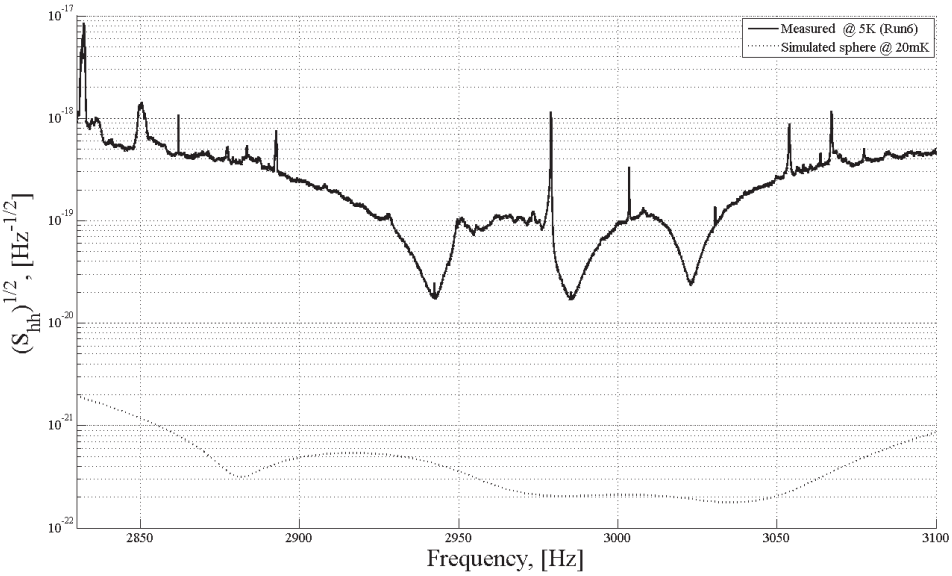

Figure 1.11**:** MiniGRAIL strain sensitivity measured at sphere temperature of 5K during cool-down in 2005 [25](solid line) and estimated average sky sensitivity using the model of the sphere with 6 transducers at temperature of 20 mK [40](dotted line)

$\sim 15Mpc$ (1 parsec $= 3.09 \times 10^{13}$ km). The estimated sensitivity for the next run on figure 1.11 is able to reach the desired level. The sensitivity is calculated using the model of the sphere presented in section 1.2.2.The model assumes that 6 transducers are placed in TIGA configuration and read out by 2-stage SQUID amplifier. The properties of the readout chain components were taken close to the realistic ones as for the status of MiniGRAIL in 2009 [32]. The thermodynamic temperature of the sphere was set to 20 mK.